Preparation of Single-Crystal "House-of-Cards"-like ZSM-5 and Their Performance in Ethanol-to-Hydrocarbon Conversion

Zhengxing Qin, Ludovic Pinard, Mohammed Amine Benghalem, T. Jean Daou, Georgian Melinte, Ovidiu Ersen, Shunsuke Asahina, Jean-Pierre Gilson, Valentin Valtchev

Preparation of Single Crystals "House-of-Cards"-like ZSM-5 and Their Performance in Ethanol-to-Hydrocarbons Conversion

*Zhengxing Qin,[a] Ludovic Pinard,[b] Mohammed Amine Benghalem,[b] T. Jean Daou,[c] Georgian Melinte,[d] Ovidiu Ersen,[d] Shunsuke Asahina,[e] Jean-Pierre Gilson,[f] Valentin Valtchev[f,g]**

[a]State Key Laboratory of Heavy Oil Processing, College of Chemical Engineering, China University of Petroleum (East China), Qingdao 266580, China

[b]Institut de Chimie des Milieux et Matériaux de Poitiers (ICM2P), UMR 7285 CNRS, 4 Rue Michel Brunet, Bâtiment B27, 86073 Poitiers Cedex – France.

[c]Université de Haute Alsace (UHA), Université de Strasbourg (UDS), Axe Matériaux à Porosité Contrôlée (MPC), Institut de Science des Matériaux de Mulhouse (IS2M), UMR CNRS 7361, ENSCMu, 3 bis rue Alfred Werner, F-68093 Mulhouse, France

[d]Institut de Physique et de Chimie de Strasbourg, Université de Strasbourg 23, rue du Loess BP 43, F-67034 Strasbourg, France

[e]SEM Application Team, JEOL Ltd., Akisima, Tokyo 196-8558, Japan

[f]Normandie Univ, ENSICAEN, UNICAEN, CNRS, Laboratoire Catalyse et Spectrochimie, 6 Boulevard Maréchal Juin, 14050 Caen, France

[g] State Key Laboratory of Inorganic Synthesis and Preparative Chemistry, Jilin University, Changchun, 130012, China

ABSTRACT

The present study reports the unbiased chemical etching of micron-sized ZSM-5 crystals with an NH_4F solution resulting in house-of-cards-like single crystals containing large rectangular cavities surrounded by thin (15 – 30 nm), flat and highly crystalline walls. The formation of such house-of-cards-like architecture is a result of the preferential extraction of mis-oriented nanocrystalline domains followed by the uniform dissolution of the remaining part of the crystal. The characteristic features of NH_4F-treated zeolites are the retention of framework composition (Si/Al) and Brønsted acidity, high crystallinity, a moderate increase in external surface area and increased accessibility to their active sites. Such a combination produces zeolitic catalysts with superior performances (activity, stability and coke resistance) in the ethanol-to-hydrocarbons conversion. The physicochemical properties of this newly engineered zeolite are compared with a hierarchical zeolite obtained by caustic leaching and zeolite nano-sheets synthesized with a bifunctional template, a di-quaternary ammonium-type surfactant.

1. Introduction

Zeolites revolutionized oil refining and petrochemistry due to their excellent chemical and (hydro)thermal stability, unique microporous structures of molecular dimensions and tunable acidity located in a shape-selective environment [1-3]. With an increasing demand for highly active and stable catalysts for existing and emerging processes, recent work with zeolites focused on morphology tailoring either during their synthesis (bottom-up approach) or by post-synthesis modifications (top-down approach), the so-called zeolite crystal engineering [4-8].

Transport limitations in their micropore channels are probably the most serious drawback of zeolite catalysts [9]. Decreasing zeolite crystal size is a straightforward approach to minimize their impact. Advances in the understanding of zeolite nucleation/crystal growth allowed the preparation of nanocrystals of many industrially important zeolites [10, 11]. However, the number of zeolite crystals synthesized with nanosized dimensions is still limited. Zeolite materials with nano-dimensions in a particular crystallographic direction were also prepared [12]. These two-dimensional microporous materials, referred to as layered- or sheet-like zeolites, offer the advantage of extended external surface areas and enhanced diffusion in a particular crystallographic direction. They were prepared, for instance, by Corma and co-workers by exfoliating layered MWW-type zeolite precursors [13]. The exfoliation approach is however limited to a few zeolites since it works with layered precursors with weaker bonds in a particular crystal direction. Ryoo *et al*. successfully synthesized a series of crystalline molecular sieves (ZSM-5 and zeolite Beta) with tunable mesostructures and nanosheet or nanosponge morphologies using amphiphilic organosilanes or multi-quaternary ammonium surfactants as bifunctional templates [14-16]. A low-cost approach to zeolite nanosheets forming “house-of-cards” structures was reported by Tsapatsis *et al.* [17]. They used a template promoting the

repetitive branching of orthogonally connected nanosheets. Such intergrowths generate structures with a mesoporous network of 2-7 nm. The resulting polycrystalline hierarchical materials offer the advantages of higher accessibility for bulky molecules, shorter diffusion pathlengths in the microporosity and a larger external surface area. At present such advanced materials were only obtained by a bottom-up approach. To the best of our knowledge, the preparation of house-of-cards by a top-down approach has not yet been reported. A post-synthesis approach to house-of-cards zeolites would provide significant advantages such as i) applicability to a large number of zeolites; ii) easy transformation of single crystals in house-of-cards materials; iii) cost and environmentally benign scaling-up to produce zeolites.

Extraction of framework cations by chemical etching has been used since the first commercial applications of zeolites (*eg.* hydrocracking, fluid catalytic cracking [FCC], isomerization…) to alleviate these ever-present mass transport limitations. For instance, high-temperature (> 600°C) steaming extracts aluminum from zeolite frameworks and redistributes it in extra-framework positions; while the overall Si/Al is unchanged, the framework Si/Al increases and rearrangement of framework Si generates a secondary mesoporosity [18]. Recently, caustic leaching [19-20] was extensively revisited, better understood and shown to generate secondary mesopores in high silica zeolites [21]. Chemical etching is an efficient and straightforward method to improve intra-crystalline transport and reduce diffusion barriers. However, the preferential or biased extraction of a particular framework cation (Al or Si) leads to a dissolution profile, strongly dependent on the zeolite composition and therefore difficult to control. Recently, an unbiased chemical etching was developed using NH_4F solutions [22-26]. Concentrated ammonium fluoride solutions were shown to dissolve Si and Al from zeolite frameworks at equal rates. While leaving the zeolite composition (Si/Al) unchanged, this

approach dissolves preferentially defects in zeolite crystals, such as interfaces between twin crystals, grain boundaries, lattice defects… This unbiased fluoride extraction is HF-free; moreover, the biased $(NH_4)_2SiF_6$ processing of zeolites is currently used in the commercial production of modified (dealumination and subsequent healing by silication) FAU zeolites (LZ-210 from UOP LLC. [27-28])

The objective of the present work is to develop a universal top-down approach to produce single crystals house-of-cards-like zeolite catalysts. It is based on the recently discovered mosaic structure of zeolite crystals, *i.e.*, the presence of rectangular nanocrystalline domains with well-defined grain boundaries [24]. Such domains were observed in MFI [24], FER [29], FAU [30], and appear to be ubiquitous. They are preferentially dissolved when an unbiased chemical etching is applied to zeolite crystals, leaving behind rectangular cavities several tens of nanometers wide. The remaining part of the crystals dissolves with a similar rate of dissolution following the morphology of extracted nanocrystalline domains, which is employed in the present study to form a house-of-cards-like material by post-synthesis etching. This is illustrated by comparing the unbiased NH_4F etching of a parent (Z_P) ZSM-5 zeolite, Z_F, a Si biased caustic leaching of the same parent, Z_B [31], and zeolite nano-sheets (Z_{NS}) prepared with a di-quaternary ammonium-type surfactant acting as a bifunctional structure directing agent [32]. The Ethanol-to-hydrocarbons (ETH) conversion was used as a model reaction to evaluate the catalytic potential of these zeolites and relate it to their physicochemical properties.

2. Results and discussion

2.1 Physicochemical characteristics of the zeolites

2.1.1 XRD

The samples preparation is provided in the supporting information. The XRD patterns of Z_P (commercially available zeolite ZSM-5, the parent), Z_B (a biased caustic etching of Z_P), Z_F (an unbiased NH_4F etched derivative), and Z_{NS} (a bottom-up ZSM-5 nanosheets preparation) are displayed in Figure 1. Z_P shows sharp and narrow peaks characteristic of a highly crystalline micron-sized MFI-type material. The XRD peaks of Z_F are equally narrow and well-defined, indicating that the NH_4F etching does not impact crystallinity. Z_B shows much lower peak intensities than its parent. Some of the peaks are missing in the XRD pattern of Z_{NS}, as expected for such type of material [32].

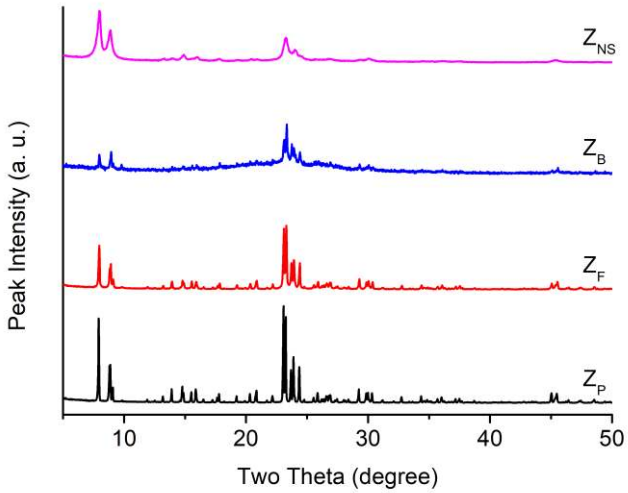

Figure 1 The XRD patterns of the parent zeolite (Z_P), its NH_4F (Z_F) and caustic (Z_B) etched derivatives, and a nano-sheet zeolite (Z_{NS}).

2.1.2 N_2 Physisorption

The physicochemical properties of all zeolites are summarized in Table 1. The parent micron-sized (Z_P) crystals display a type I isotherm (Figure S1) characteristic of a purely microporous zeolite [33]. Z_F and Z_B zeolites exhibit a second uptake and a hysteresis loop at high relative

pressure revealing the presence of mesopores. The micropore volume of Z_F is fully retained compared to its parent and its external surface area is lower than its caustic leached counterpart, Z_B; Z_B has however lost some of its micropore volume, in agreement with the XRD data. The zeolite nano-sheets, Z_{NS}, display a Type I isotherm at low p/p^0 combined with a type IV(a) at high p/p^0. The presence of a hysteresis loop in the relative pressure range $0.4 < p/p^0 < 1$ is typical for such lamellar materials due to the stacking of nanosheets. Z_{NS} also exhibits a lower micropore volume and larger external surface area. The mesopores distribution for all samples is presented in Figure 2. No mesopores are observed in the parent micron-sized crystals, Z_P. Z_F exhibits a large pore size distribution between *ca* 10 nm and more than 100 nm. The Z_B pore size distribution is also large, but within the mesopore range, *i.e.,* 2 to 50 nm [33]. The pore size distribution of Z_{NS}, with a maximum of around 6 nm, is much sharper compared with Z_B and Z_F. All three hierarchical zeolites have a mesopore volume higher than 0.3 $cm^3\ g^{-1}$ (Table 1). However, Z_F shows only a slight increase in external surface area compared to its parent. Conversely, Z_B and Z_{NS} both develop external surfaces exceeding 200 $m^2\ g^{-1}$. We attribute these differences to the types of pores formed by NH_4F and caustic leaching and the stacking of nanosheets, respectively. The dissolution in fluoride medium results in the formation of large meso- and macropores (Figure 2), which exhibit low specific surface area (Table 1). This can be further interpreted based on a rough estimation of the relation between the surface (*S*), the pore diameter (*d*) and the pore volume (*V*) using $d = 4V/S$. In contrast, both Z_B and Z_{NS} contain a substantial amount of small mesopores with size below 10 nm (Figure 2). Accordingly, a substantial increase in the external surface area is observed (Table 1).

Table 1. Physicochemical characteristics of the series of ZSM-5 samples.

Samples	Si/Al[a]	S_{BET}[b]	S_{ext}[c]	V_{mic}[c]	V_{meso}[d]	B_{Py}[e]	L_{Py}[e]
		$m^2\ g^{-1}$	$m^2\ g^{-1}$	$cm^3\ g^{-1}$	$cm^3\ g^{-1}$	$\mu mol\ g^{-1}$	$\mu mol\ g^{-1}$
Z_P	21	377	9	0.18	0.02	617	91
Z_F	22	395	54	0.17	0.31	582	51
Z_B	9	494	206	0.13	0.36	495	282
Z_{NS}	37	504	266	0.11	0.40	162	98

[a]ICP. [b]BET surface area. [c]*t*-plot. [d] $V_{meso} = V_{total} - V_{mic}$ (V_{total}: the volume absorbed at p/p^0 = 0.99). [e]The Brønsted (B_{Py}) and Lewis (L_{Py}) acidity were determined by IR analysis of pyridine sorption.

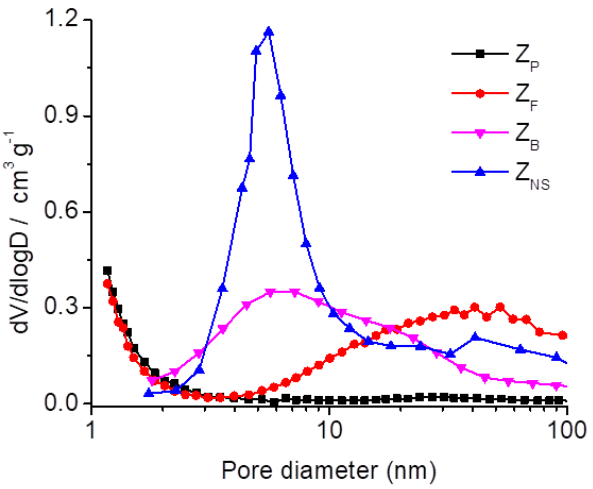

Figure 2. BJH pore size distribution of the parent zeolite (Z_P), its NH_4F (Z_F) and caustic (Z_B) etched derivatives and the nano-sheet zeolite (Z_{NS}).

2.1.3 Morphological analysis

The morphology and secondary porosity of the zeolites are described by combining scanning (SEM) and transmission electron microscopy (TEM). NH_4F etching transforms the micron-sized ZSM-5 crystals (Figure 3a, insert) into a foam-like material with thin crystalline walls (Figure 3a, b). The macro-morphological features of the crystals are retained. However, the crystalline body is fully transformed into a mosaic of rectangular cavities, large enough to be observed with a scanning electron microscope (Figure 3a, b). TEM provides further insights into the structure and morphology of the NH_4F etched zeolite. Figure 3c shows a representative TEM image of such an NH_4F etched ZSM-5 crystal. Figure 3e-g show slices through the electron tomography reconstruction of a selected zeolite grain. The slices highlight the high porosity of chemically treated zeolite but also the remained crystalline pore walls (Figure 3d) with a thickness ranging from 10 to 30 nm. The tomography shows that the NH_4F etched zeolite contains two types of secondary pores: i) large interconnected rectangular-shaped, ii) smaller ones probably formed later on during the etching. 3D models indicate that even the vast majority of the smaller mesopores are connected to the secondary porous network, indicating that pore connectivity approaches 100 % and an overall meso-macroporosity of around 47%. This excellent connectivity between the various pore networks is an important, albeit often overlooked, feature in hierarchical zeolites [34]. The porosity could even be higher as some of the surface pores (Figure S2) were excluded from the quantification. The 3D geometry of the porous network and their walls resemble the “house-of-cards” architecture. A schematic presentation of the remaining part of the crystals with the vast sytem of rectangular, interconnected cavities is presented in Figure S3. It is remarkable that such a significant secondary porosity increase in Z_F is achieved without loss of intrinsic microporosity and acidity (Table 1) as well as crystallinity (Figure 1, Figure 3d).

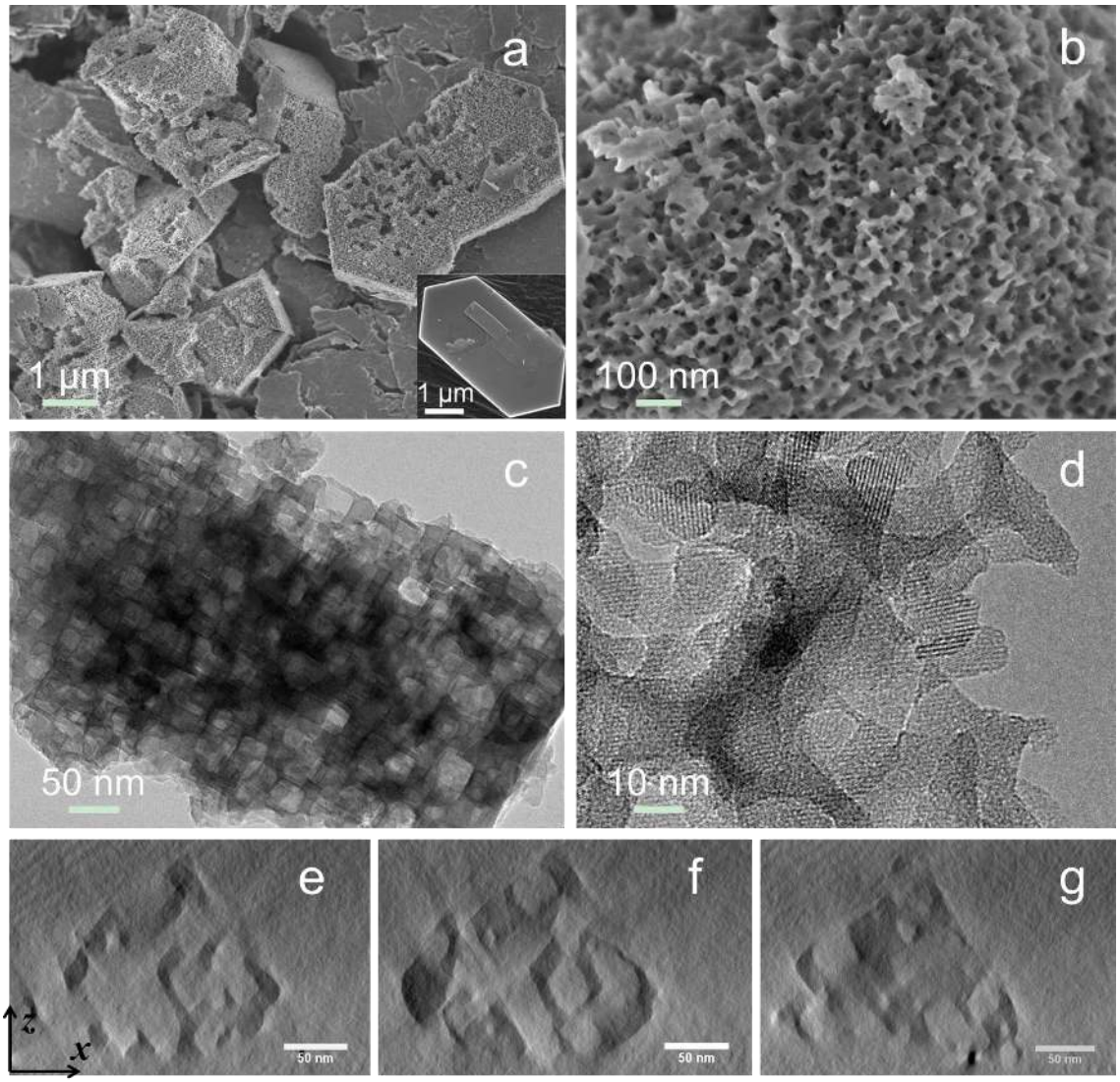

Figure 3. Low (a) and high (b) resolution SEM images of Z_F sample. Representative low (c) and high (d) resolution TEM images of Z_F. TEM tomography slices in *zx* direction (e, f, g).

Zeolite dissolution process is strongly influenced by the zeolite framework composition and crystal zoning in the case of selective chemical extraction of a framework cation [35–37]. The NH_4F did not show any sensibility to the framework ratio, including in the case of very low silica

zeolites [25, 26]. Indeed the Z_F sample shows a Si/Al ratio very similar to its parent (**Table 1**). For this reason, we consider that the exceptional resistance of the periferic parts of the crystals to the NH_4F etching (Figure 3a, Figure S4, S5) is an important observation. In order to get a deeper insight into this peculiar "selected-area" dissolution behavior, a comparative study was conducted by combined use of high and low voltage SEM. The electron beam penetrates deep into the sample at high accelerating voltage. Accordingly, the signal will carry information from deeper layers of the sample. In contrast, low voltage high resolution SEM provides only the surface information thanks to the much lower landing voltage [38]. Therefore, as the intensity of the generated secondary electrons varies depending on the magnitude of the accelerating voltage, variations in the roughness of specimen surface and the density of the substance can be detected. As can be seen in Figure S6, the crystal surface of Z_P shows a uniform contrast under both high and low voltage observation models. The 5 min NH_4F-treated sample also shows a uniform contrast under the low voltage observation model (Figure S7a). In the case of the high voltage model, however, obvious dark areas occur on the *b* crystal face of the NH_4F-treated sample (Figure S7b). This contrast difference is not related to crystal surface etching (i.e. surface roughness), since only a few seperated holes can be observed on the *b* crystal face (**Figure S8e**). This crystal surface still shows a similar smouth morphology as the untreated sample, with the growth steps clearly distinguishable (Figure S8b, e). In addition, the difference in surface contrast is not an individual but a general phenomenon, as a similar inhomegeneous distribution of the phase contrast was also observed in case of the 10 and 20 min NH_4F-treated samples (Figure S9). The surface contrast is not so different in the case of the longer time (i.e. 30 and 60 min) treated samples (Figure S10). In the later case the original crystal surface are either deeply

etched, or detached as a result of the substantial dissolution of the inner part of zeolite crystals (Figure S11).

Based on these intensive SEM observations, we attribute the difference in surface contrast to the difference in density in different parts of zeolite crystals. Namely, the dissolution of zeolite crystals in NH_4F solution is spacially inhomogeneous in the macro sense. In general, the inner part of zeolite crystals are preferentially dissolved. The gravimetric measurement of the weight loss of zeolite with the extension of NH_4F etching was also conducted (Figure S12). The continuous decrease of the slop of the weight loss curve shows unambiguously that the dissolution of the Z_P crystals is relatively faster at the initial stage and the dissolution rate slows down with increasing etching time (Figure S12). We further attribute the faster dissolution of the inner part to the fast growth rate at the early stage of crystal growth, and the slower dissolution of the crystal periphery to the slow growth rate at the end of the crystallization process where a few defects are formed. Thus the defect-poor parts of the crystals are resistant to the etching. This result is additional evidence showing that the dissolution starts preferentially from framework defects when unbiased etching solution is used.

The relation between the crystallographic structure of the zeolite crystals and the etching direction shown in Figure S4 is confirmed by the high-resolution analysis of some similar grains. Figure S13 shows a typical high-resolution TEM image and the corresponding FFT pattern which illustrate that the preferentially etched facets are on {010} face, as revealed also by the low-magnification TEM images of the various analyzed zeolite crystals. It should be underlined that the empty cages resulting from the crystal dissolution are orianted along the crystallographic axes. This is a proof for the connection between the growing process and dissolution behaviour

of the crystals. The high-resolution image shown in Figure S14 also sustains this important finding.

We attribute both the spacially inhomegeneous dissolution and the facet-dependent etching behavior to the growth mechanism. The fluoride etching is sensitive solely to the zones of structural stress and deffect concentartion (Figure S8d) which are more vulnerable to chemical attack [24, 39, 40]. Thus the dissolution reflects the particularities of the growth process. Layer type growth is characteristic of most of the zeolitic materials [41–44]. The detailed mechanism of MFI growth was revealed recently by in situ AFM microscopy [43]. It was observed that the MFI growth involves two simultaneous phenomenon - oriented attachment of nanoparticle and mono- or low-weight silica species. The nanodomains integrated into the growing crystal contain well defined grain boundaries and thus are rapidly disolved by NH_4F etching (Figure S8c, f), leaving behind rectangular cages [24]. These rectangular cages are surrounded by crystalline material, which is a result of the uniform growth by means of low weight silica species. The rate of dissolution of this more stable and uniform part of the crystal is lower (Figure S12). Judging by the straight and flat crystalline walls surrounding the cages the dissolution can be described as "layer-by-layer" process. The results of the present study show that the mechanism of dissolution does not change with the time of treatment and thus a house-of-cards-like material can be synthesized. A fundamental feature of this material is that each "house-of-cards" is a single crystal thanks to the preferential removal of defect-rich zones (Figure 3c). Electron diffraction is a very appropriate technique for the assessment of the crystallinity of various types of specimens at the nanometer level. As shown in Figure S15, the ZSM-5 grains give rise to a unique set of well-defined diffraction spots, allowing us to assign to these crystals a single crystalline structure. In contrast to the interpenetrated "house-of-cards" with myriad intergrown plane

prepared by a bottom-up approach, the single crystal house-of-cards-like material reported here offers highly crystalline with a few frameworks defects left.

In order to shed light in the dissolution process and the general applicability of the method, we have employed a series of industrial ZSM-5 sample (see Supporting information). These samples exhibit different morphology and particle size (Figure S16), Si/Al ratio (Table S1) and level of aggregation. The samples were NH_4F etched under similar conditions as the time of treatment was varied between 5 and 50 min. The product yield ploted against the etching time is presented in Figure S12. As can be seen, the dissolution rate depends on the crystal size, the larger the crystal size, the lower the dissolurion rate is. We relate this result with the accomplishement of the growth process. As discussed, the well shaped crystals with terminated crystal faces show higher resistnace to the NH_4F etching. On the other side, all the trend lines show an initially faster dissolution rate and then converge, with an apparently lower dissolution rate, to a similar product yield value under the applied experimental conditions. This result shows that no matter of basic zeolite crystal characteristics, the mechanism of dissolution is identical and the final product is similar (Figure 3, Figure S17).

The silicon selective alkaline etching also leads to a hierarchical zeolite, Z_B (Figure 4a, b). It is a highly porous material with large variation of mesopore size and pore distribution [31, 35]. Similarly to NH_4F etching, the crystal morphology is retained (Figure 4a). However, a closer look reveals a grain-like morphology (Figure 4b), the result of preferential Si extraction and re-deposition of most of the extracted Al on the etched surface. Such a biased Si etching changes the zeolite framework composition and acidity (Table 1).

Z_{NS} displays a flower-like morphology composed of interpenetrating plate-like nanosheets (Figure 4c, d). The overall thickness of the lamellar stacking of nanosheets is 20–60 nm (Figure 4e). TEM reveals that the stacking "plate" is composed of alternating 2 nm-thick aluminosilicate nanosheets and 2.8 nm micellar layers (Figure 4f). This well-defined mesoporosity is inherently related to the properties of the structure-directing agent used.

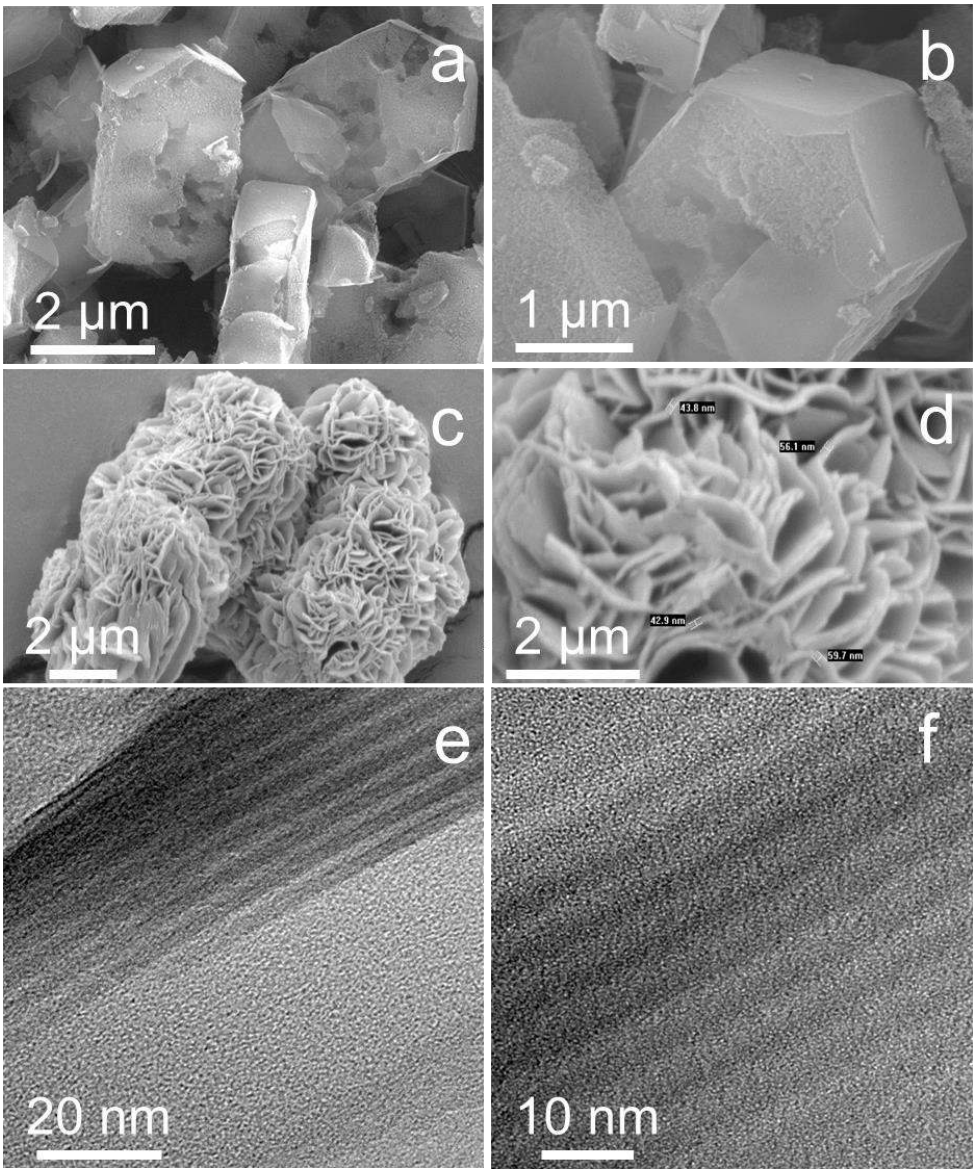

Figure 4. Low (a) and high (b) magnification of SEM micrographs of caustic etched ZSM-5 crystals, Z_B. Low (c) and high (d) magnification images of ZSM-5 nanosheets (Z_{NS}) prepared by a bottom-up approach. TEM images representing the overall thickness of zeolite lamellas (e) and high-resolution micrograph of ZSM-5 nanosheets building the nanosheet sample (f).

2.1.4 IR spectroscopy

Chemical analysis of Z_P and Z_{NS} indicates Si/Al ratios of 21 and 37, respectively. A negligible change in the Si/Al ratio after NH_4F etching is observed, while caustic etching produces a material with a Si/Al ratio of 9 (Table 1). These results are expected for unbiased (NH_4F) and biased (NaOH) etchings, respectively [23]. IR spectroscopy of adsorbed pyridine highlights further these conclusions as Z_B has a lower concentration of Brønsted acid sites and a substantial increase of Lewis acid sites compared to its parent Z_P and its NH_4F etched derivative Z_F (Table 1). Z_F Brønsted acidity does not change significantly, as excepted. Z_{NS} has a lower Brønsted acid sites concentration, due to a higher Si/Al ratio and the presence of numerous silanols, *vide-infra* [44]. The pristine surface of all samples can also be probed by FTIR spectroscopy, namely their $\nu_{(OH)}$ region where isolated silanols (3747 cm^{-1}) located on the external surface and bridged hydroxyls, *i.e.* Brønsted acid sites (3613 cm^{-1}) are clearly observed (Figure 5). Z_P shows such bands and a broad absorption extending from 3500 to 3000 cm^{-1} (Figure 5a), ascribed to H-bonded internal silanol nests [45]. The Z_F spectra does not show such a broad band, and the baseline is almost flat, indicating that a substantial part of the silanols is eliminated during NH_4F etching. Again, this is the result of a preferential dissolution of highly defective zones in the crystals, a typical characteristic of NH_4F etching [24, 40]. In Z_F, the intensity of the 3747 cm^{-1}

band increases compared to its parent Z_P, indicative of an increased external surface area (Table 1). For Z_B, the intensity of the 3747 cm^{-1} band further increases while 3613 cm^{-1} band decreases noticeably. The IR spectra of Z_{NS} is dominated by external surface silanols at 3743 cm^{-1} (Figure 5a) while a very small amount of Brønsted acid sites is detected (Figure 5b).

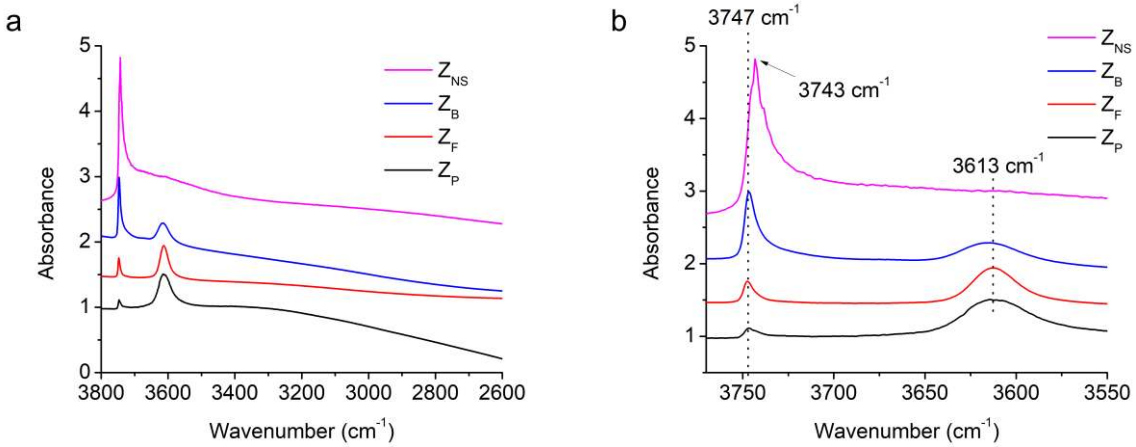

Figure 5. IR spectra of Z_P, Z_F, Z_B, and Z_{NS} in the 2600-3800 cm^{-1} $\nu_{(OH)}$ region (a) and zoom on the $\nu_{(OH)}$ (3550-3770 cm^{-1}) region (b).

The above results indicate that a ZSM-5 house-of-cards-like architecture, Z_F, can be prepared by a top-down unbiased NH_4F etching of ZSM-5. Single zeolite crystals are converted in a mosaic of connected rectangular cavities separated by nanometer thick crystalline walls. Such walls are thicker than the house-of-cards obtained by a bottom-up approach, Z_{NS} (Figure 3e-g and Figure 4e, f). However, the aspect ratios between the wall thickness and mesopore space of both Z_F and Z_{NS} are similar. As mentioned, the formation of rectangular cavities is a consequence of the unbiased dissolution of highly defect zones and small crystalline domains mostly presented in zeolite crystals. Thus, an essential advantage of the top-down approach is

that the "house" is a single crystal almost free of defect zones. A decrease of Lewis acid sites is observed, again a consequence of the preferential dissolution of defective portions of the crystals (Table 1) while the number of Brønsted acid sites is almost unchanged. The resulting house-of-cards-like material comprises relatively large meso- and macro-pores with a flat surface. Another essential feature of the house-of-cards-like material is the moderate increase in external surface area and retention of micropore volume compared to the caustic leached ZSM-5. Nanosheet-like ZSM-5 also shows relatively low micropore volume. Z_F differs substantially from the caustic leached zeolite produced from the same parent (Z_B) and the nanosheet ZSM-5 (Z_{NS}). In contrast, the preferential extraction of Si and redeposition of Al in the case of Z_B results in a considerable increase of the external surface area at the expense of the micropore volume, dramatic changes in the chemical composition and the acidic properties of the zeolite (Table 1). Nanosheet ZSM-5 also exhibits a huge external surface area and reduced micropore volume. It should be noted the very low Brønsted acidity of this material (Table 1) and the vast presence of surface silanols in this material (Figure 5). This series of catalysts with well distinct physicochemical properties offers the possibility a structure-property relationship to be established.

2.2 Ethanol-to-hydrocarbons (ETH) conversion on Z_B, Z_F, and Z_{NS} zeolite catalysts

ETH, like the methanol-to-hydrocarbons (MTH) process, is a key step in the transformation of biomass, coal, natural gas, heavy oils into olefins (major building blocks in petrochemistry) and higher hydrocarbons (gasoline fuel) [46]. The performance of all these four zeolites is evaluated in this reaction as already discussed previously [31]. Ethanol is converted into water and light olefins as well as heavier hydrocarbons (3 to 18 carbon atoms). Small amounts of methane and ethane are detected but no CO and CO_2. The yields are presented as molar % in the organic fraction (Figures 6 and 7). While ethanol dehydration can take place on weak acid sites,

oligomerization, cyclization and hydrogen transfer reactions require strong acid sites as found in zeolites. On all our catalysts, ethanol conversion is initially complete and decreases slowly with time-on-stream (Figure S18a). Therefore, the catalyst deactivation is related to the time evolution of the C_{3+} yield.

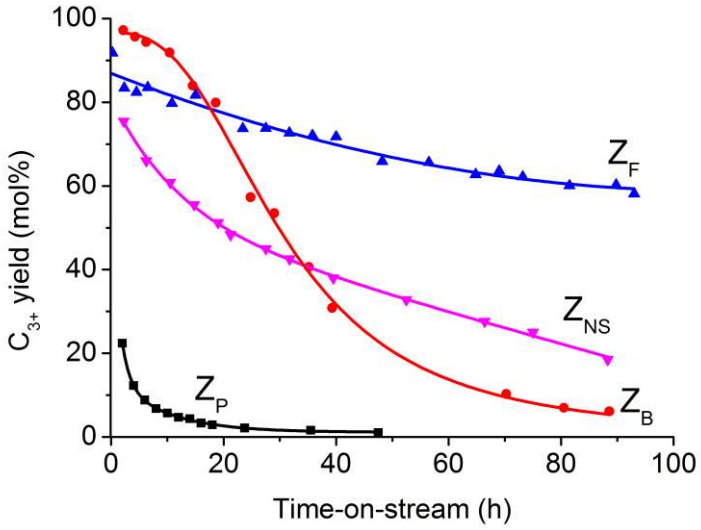

Figure 6. Molar yields of C_{3+} hydrocarbons as a function of time-on-stream during the conversion of ethanol at 623 K and 3.0 MPa on Z_P, Z_F, Z_B, and Z_{NS} zeolite catalysts. The lines are drawn simply to guide the eyes.

On the parent zeolite (Z_p), the initial yield of C_{3+} is only 35 % (extrapolated value at zero conversion) and decreases rapidly becoming negligible after only 20 h (Figure 6). On Z_B, the initial C_{3+} yield is slightly less than 100% (Figure 6), but the catalyst deactivates rapidly and yields almost no C_{3+} after 90 h on stream. On Z_{NS}, the initial C_{3+} yield is lower than Z_B but quite high considering its much lower Brønsted acid site concentration. However, its deactivation rate

is much lower than Z_B: after 90 h on stream, the C_{3+} yield decreases to *ca.* 20 mol.% while it was almost zero on Z_B. The direct synthesis of a hierarchical zeolite using a complex surfactant is an efficient, albeit expensive, way of minimizing deactivation. Z_F, although not the catalyst with the best initial C_{3+} yield retains it much longer as it deactivates much slower than Z_B and Z_{NS} (Figure 6); after 90 h of TOS, it still produces a substantial C_{3+} yield, *ca.* 60 mol.%.

The unbiased NH_4F etching of a micrometer-sized ZSM-5 zeolite leads to a diffusion path length similar to that of nanosized one. Indeed, the stability of Z_F is similar, or even higher for longer reaction time, to that on a commercial zeolite with a crystal size of 45 nm [31]. See also Figure S19 in the present work. The superior stability of Z_F on a nanoscale zeolite can be related to both a high intracrystalline mesoporous volume (0.31 $cm^3.g^{-1}$) and quasi-perfect connectivity with the microporous network, a consequence of single crystal nature of house-of-cards-like material. As Z_F is devoid of defects, contrariwise on Z_{NS}, the immobilization and growth of coke precursors are mitigated. Therefore the catalyst is more stable. On the other hand, as the caustic leaching divides by only four the diffusion path length as shown by the desorption experiments [47], the gain in stability is rather limited.

The molar yields of the paraffins (P), olefins (O), naphthenes (N), and aromatics (A), as well as the paraffins to aromatics molar ratio (P/A), are reported as a function of the C_{3+} yield and time-on-stream in Figure 7 and Figure S18b-f, respectively. As far as product distribution is concerned Z_P, Z_{NS} and Z_P give the same product selectivity for the same C_{3+} yield, meaning that the reactions involved are identical, even during the deactivation and regardless of the acid properties of the three catalysts. It is worth to note that a difference exists only on Z_B with a yield in O_{3+}. Yields in N and O_{3+} pass through a high yielding maximum in C_{3+}, while those in P and A increase exponentially. Regardless of C_{3+} yield the paraffins to aromatics molar ratio (P/A) is

ca. 3 (Figure 7e), indicative of hydrogen transfer between naphthene and olefins (Scheme 1). The initial low value of P/A ratio (open symbol in figure 7e) is due to coke formation.

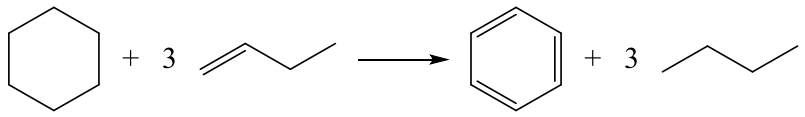

Scheme 1. The hydrogen transfer reaction between naphthene and olefins.

In sharp contrast, Z_F shows considerably higher aromatic and naphthene yields than Z_B and Z_{NS}, while its paraffin yield is low (Figure 7a, c, d). Apparently, hydrogen transfer reactions are substantially suppressed in this catalyst. Its P/A is lower than 0.5 (Figure 7e), implying that on the NH_4F treated zeolite, aromatics are formed by a monomolecular protolytic dehydrogenation. Lercher and coworkers [48] have shown that a high ratio of Brønsted acid sites to Lewis acid sites (BAS/LAS) minimizes the alkenes concentration and causes high hydride transfer (HT) activity. Yet on Z_F catalyst, HT is limited although the house-of-cards-like catalyst possesses the highest BAS/LAS ratio. Lercher et al. [49] also demonstrated that the rate determining step for dehydrogenation activity of alkane on H-ZSM-5 is represented by olefin desorption from the catalyst surface which is promoted by a short diffusion path length. It is worth mentioning that the products selectivity of Z_F is very close to nanometer-sized ZSM-5 zeolite (Figure S20), confirming that the diffusion path length is limited to a few nanometers on both zeolites.

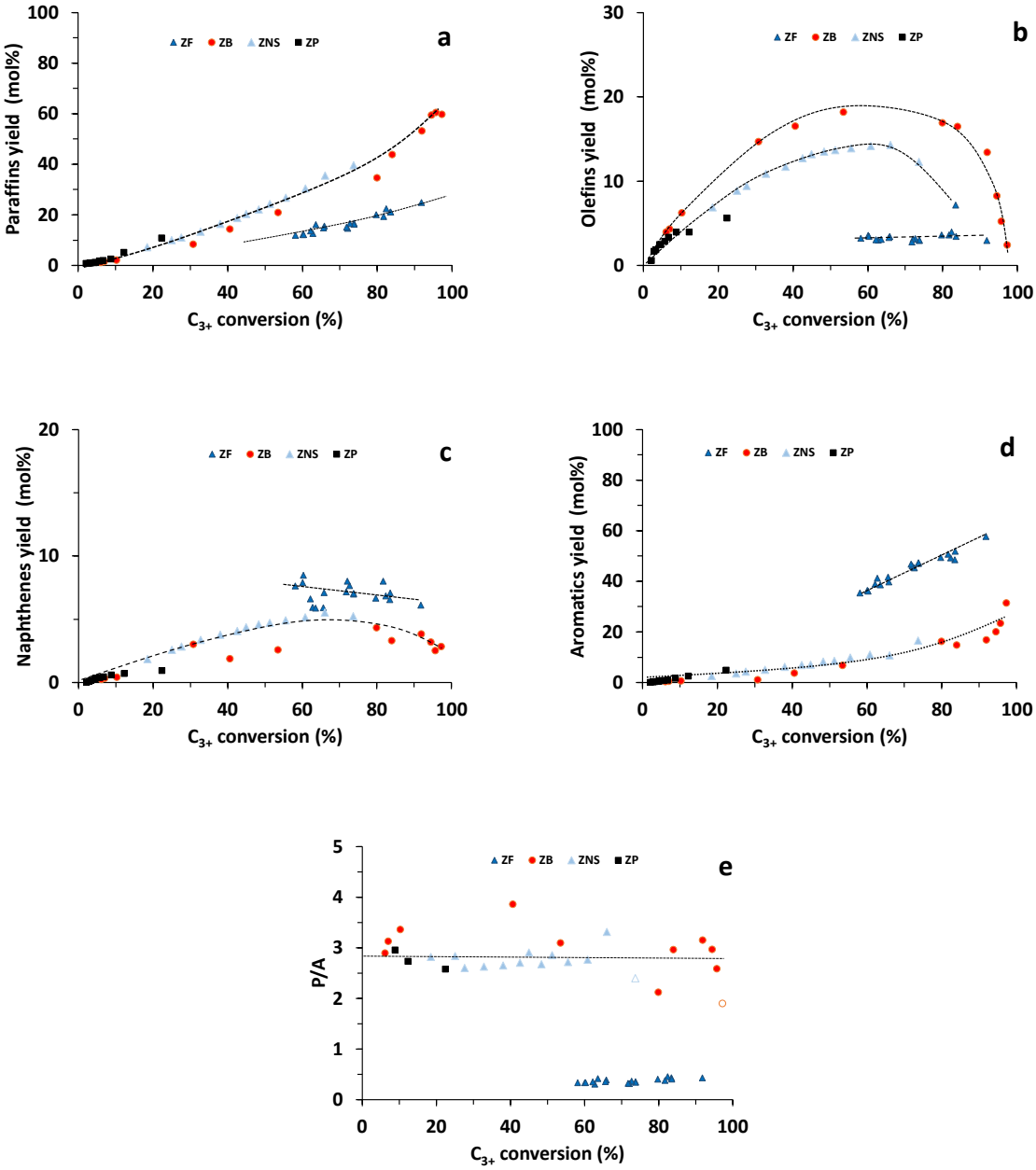

Figure 7. Ethanol transformation at 623 K and 3.0 MPa on Z_P, Z_F, Z_B and Z_{NS} zeolite: (a) molar yields of paraffins (P), (b) olefins (O_{3+}), (c) naphthenes (N), (d) aromatics (A), and (e) molar P/A ratio catalysts as a function of C_{3+} conversion. The lines are drawn simply to guide the eyes.

The coke content, the evolution of the number of acid sites (Brønsted and Lewis) and pore volumes accessible to nitrogen after more than 48 h of reaction are gathered in Table 2. The coke

content is around 13 wt % on Z_P after 48 h of reaction. NH_4F etching has no impact on the coke level, while on the alkaline leached Z_B catalyst, coke grows continuously to reach a level almost twice as high as its parent. On Z_{NS}, although its Brønsted acid site concentration is 4 times lower than on Z_P, coke content is quite similar. The residual acidity (Brønsted and Lewis), after deactivation, is very low for all samples. An important decrease of micropore volume occurs on all zeolites. On Z_{NS} which is the least acidic catalyst, the loss of microporosity is only 25%. The coked Z_F and Z_{NS} catalysts, despite a near total loss of acidity, keep converting ethanol to C_{3+} hydrocarbons (~60 %, and ~20 %, respectively, (Figure 6)); ethanol transformation occurring probably by pore mouth catalysis on hybrid active sites (immobilized carbocations) by a carbon pool mechanism [31].

Table 2: Coke content, T_{50} and T_{90} (temperatures required to remove, by combustion, 50% and 90% of coke respectively), pore volumes and acidity of Z_P, Z_F, Z_B and Z_{NS} zeolite spent catalysts.

Samples	Time	Coke	T_{50}	T_{90}	V_{mic}[a]	V_{meso}[b]	B_{Py}[c]	L_{Py}[c]
	h	wt%	°C	°C	$cm^3\ g^{-1}$	$cm^3\ g^{-1}$	$\mu mol.g^{-1}$	$\mu mol\ g^{-1}$
Z_P	48	12.9	615	705	0.01	0.02	4	5
Z_F	90	12.5	560	670	0.05	0.13	1	10
Z_B	110	20	580	680	0.03	0.36	2	14
Z_{NS}	90	10.5	560	665	0.08	0.17	0	14

[a] *t*-plot. [b] $V_{total} - V_{mic}$ (V_{total}: the volume absorbed at $p/p^0 = 0.99$). [c] The Brønsted acidity (B_{Py}) and Lewis acidity (L_{Py}) determined by pyridine sorption.

Differences in the activity and stability between Z_P, Z_B, Z_F, and Z_{NS} are related to changes in the carbon pool composition. The composition of the coke trapped in the zeolite micropores, *i.e.*,

internal coke, is determined by mineralizing the zeolite and subsequently analyzing the organic phase after a liquid-liquid extraction with CH_2Cl_2 [50]. Coke molecules can be lumped in four families according to their number of aromatic rings: alkylbenzenes (I), alkyl naphthalenes (II), alkyl-phenanthrenes or -anthracenes (III) and alkylpyrenes (IV). The sizes of all compounds trapped in the micropores vary between the dimensions of the pore openings (0.55 nm) and channel intersections (~1 nm) of H-ZSM-5. The coke on Z_P and Z_B contain representatives of all families. A simpler and lighter coke distribution is found on Z_F and Z_{NS}, where families I and III dominate (Figure S21); such a coke composition is similar to that reported elsewhere on nano-sized zeolite [31]. The average molar mass of coke trapped in the micropores, calculated from these compositions, is 200 g mol^{-1} for Z_P and Z_B, and 180 g mol^{-1} for Z_F and Z_{NS}.

Taking this average molar mass of 200 g mol^{-1} for the coke molecules trapped inside the micropores (*ca.* 13 wt % on the Z_P catalysts), its concentration is *ca.* 645 mol g^{-1}, corresponding to the amount of Brønsted acid sites on the fresh zeolite. Coking is therefore mainly a site poisoning effect, further confirmed by a complete disappearance of the bridged OH groups (Figure S22). Assuming that on all hierarchical zeolites, one coke molecule poisons only one protonic site, the coke trapped within the micropores and that located in the mesopores can be estimated. The results are reported in the bar chart on Figure 8. The most significant accumulations of coke on the mesopores are for the caustic leached micron-sized zeolite (Z_B) and the nanosheet zeolite (Z_{NS}), reaching up to 55% and ca. 75% of the total coke, on the other hand, it is limited to 16% on the catalyst free of defect (Z_F) and as expected, almost zero on the parent zeolite. The accumulation of coke in mesopores is likely related to the quality of the crystals. The increased number of silanols and Lewis acid sites on Z_B and Z_{NS} are prone to trap desorbed products [51–53] as confirmed by the disappearance of silanol groups on spent catalysts (Figure

S22). Taking a coke density of 1.1 g cm^{-3}, the volume of coke in the micropores corresponds to the loss of micropore volume measured by nitrogen adsorption (Figure 8). These calculated values are very close to the experimental data, highlighting the relevance of this procedure to discriminate between internal and external coke contents.

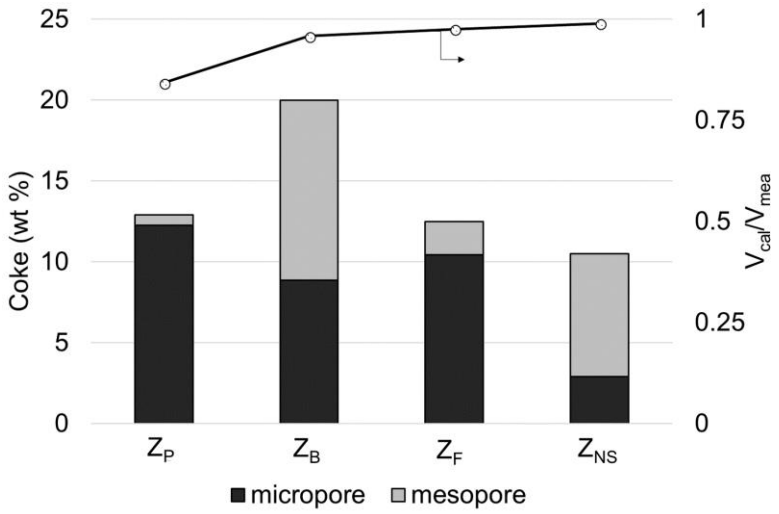

Figure 8. Estimation of the coke distribution between micropores and mesopores on Z_P, Z_F, Z_B and Z_{NS} zeolite spent catalysts

In addition, the coke light-off performances of the spent catalysts are compared in Table 2 where temperatures required to combust 50% (T_{50}) and 90% (T_{90}) of the coke are reported. T_{50} and T_{90} are both lower on Z_B than on Z_P (-35 °C and -25 °C respectively) and much lower on Z_{NS} and Z_F (-55 °C). The differences are related to a higher accessibility (difusion) of oxygen to the coke molecules trapped in the micropores. The house-of-cards-like zeolite, already the best

catalyst (cumulative performance due to its time stability) is as good as a nanosheet one for regeneration.

The ETH reaction illustrates the superior stability and selectivity of Z_F, a house-of-cards-like ZSM-5 catalyst, although other hierarchical zeolites, Z_B and Z_{NS} possess higher external surface area and mesopore volume. The nano-sheet zeolite Z_{NS} with a higher Si/Al ratio of 37 and lower acid site density displays a remarkably high initial C_3^+ yield and was once expected to be a superior candidate for ETH reactions [54] but lacks stability as shown in this study. The Z_F catalyst outperforms both Z_B and Z_{NS} in the present study, but the Z_{NS} hierarchization procedure brings superior performances than a micron-sized zeolite, Z_P (Figure 6). Zeolite acidity and mesoporosity cannot alone fully explain the differences in catalytic performances discussed above. Based on our detailed comparison of the hierarchical zeolites, we propose that, in addition to mesopore size, shape, uptake capacity and connectivity, the quality of the hierarchical zeolites (micropore accessibility, absence of defects [silanol nests], Lewis acidity) also play important roles in the ETH reaction. The higher catalytic performances of NH_4F leached zeolites could also be related to their ability to dehydrogenate naphthenic compounds (Figure 7); this monomolecular reaction requires less space than the bimolecular hydrogen transfer occurring on the caustic leached zeolite and nano-sheet zeolite. The absence of defects combined with a small diffusion pathlength inside the microporosity by retarding the transformation of the desired active carbon pool to unwanted coke, slows catalyst deactivation. The presence of numerous silanol groups, on the other hand, traps coke precursors on the surface, promoting a rapid catalyst deactivation by a fast accumulation of aromatic compounds. Indeed, as coke formation is a genuine shape selective reaction, the availability of more space favors the production of larger molecules, coke, *i.e.* an inactive carbon pool. These results highlight that, in addition to the

loosely defined “mesopore quality” [21], the surface quality of the remaining microporous crystal domains determines the catalytic performance of hierarchically structured zeolite crystals.

Conclusion

Single house-of-cards-like ZSM-5 crystals were prepared by a top-down approach using a novel unbiased chemical etching with an NH_4F solution. Such an etching extracts Si and Al at similar rates and preferentially removes less-stable defect zones in the crystals. The process is therefore controlled by the number of intergrowths, the structural stress and the nanocrystalline domains with well-defined grain boundaries, *i.e.* the history of the zeolite synthesis. Such a unique dissolution behavior is inherently related to the growth process where simultaneous monomer-by-monomer addition and oriented attachment take place [42]. The unbiased NH_4F dissolution leads to the preferential extraction of misoriented and more vulnerable to chemical attack nanocrystalline domain followed by progressive etching of the remaining part of the crystals, which is more resistant due to the limited number of structural defects. This dissolution proceeds by a layer-by-layer mechanism following the rectangular features of previously extracted nanodomains, thus the well shaped cavities grown in size and connect each other providing a house-of-cards-like morphology.

Such a hierarchical material is analogous to a collection of nanosized high quality crystals with the same framework composition and Brønsted acidity of their parent. The high accessibility and short diffusion pathlength offered by the house-of-cards-like morphology is therefore combined with the intact native microporosity and acidity of their parent zeolite and does not require expensive and one-off structure directing agents. The optimization of structural and chemical parameters results in an excellent catalyst easier to regenerate, as demonstrated in the

challenging (deactivation prone) ethanol-to-hydrocarbon reaction. Indeed, regenerating deactivated catalysts by controlled coke combustion often leads to, often overlooked, irreversible changes due to the operating conditions (such an exothermic reaction produces steam near the zeolite active sites and can lead to structural and chemical damages such as dealumination) of this step. The performance of such single crystals house-of-cards-like catalysts is so far second to none as it maintains its performance over longer periods of time and appears easier to regenerate, which even outperforms the nanometer-sized zeolites (Figure S19). Noting that we have previously concluded, based on the samples studied, that the reduction of crystal size is the most efficient way to increase the performance of zeolites for applications such as alcohols to hydrocarbons, and hence nano-zeolites are preferred [31].

This study highlights that hierarchical zeolitic catalysts with superior performances can be designed not only by promoting high accessibility and short diffusion to and from their active sites, but also by retaining the crystallinity and acidity of their parents while keeping a minimum level of defects. Since the presence of crystalline domains with well-defined grain boundaries is a ubiquitous in zeolite materials, the preparation of single crystal house-of cards can be extended to other zeolite types. Further insights in the hierarchization process of zeolites, either bottom-up or top-down (this work) hold much potential to design ever bettter zeolite catalysts for current and forthcoming applications [55].

Supporting Information. Experimental details, the nitrogen physisorption isotherms, the combined 3D models of zeolite body and pores, the additional SEM and TEM images and a graphical representation of the house-of-cards-like architecture, the additional data of the

Ethanol-to-Hydrocarbons reaction, coke composition by GC analysis, and the IR spectra of the coked zeolite samples.

Corresponding Author

*valentin.valtchev@ensicaen.fr

ACKNOWLEDGMENT

Zhengxing Qin acknowledges funding support from NSFC 21706285, China University of Petroleum (East China) starting funding, and the Fundamental Research Funds for the Central Universities (18CX02013A). ZQ, JPG and VV acknowledge funding from the French-Sino International Laboratory (LIA) “Zeolites”.

REFERENCES

[1] Martínez C.; Corma A. Inorganic molecular sieves: Preparation, modification and industrial application in catalytic processes. *Coordination Chemistry Reviews* 2011, 255, 1558-1580.

[2] Vermeiren W.; Gilson J.-P. Impact of Zeolites on the Petroleum and Petrochemical Industry. *Topics in Catalysis* 2009, 52, 1131-1161.

[3] Vogt, E. T. C.; Weckhuysen, B. M. Fluid catalytic cracking: recent developments on the grand old lady of zeolite catalysis, *Chemical Society Reviews* 2015, 44, 7342-7370.

[4] Tosheva, L.; Valtchev, V. Nanozeolites: Synthesis, Crystallization Mechanism, and Applications. *Chemistry of Materials* 2005, 17, 2494-2513.

[5] Valtchev, V.; Tosheva, L. Porous Nanosized Particles: Preparation, Properties, and Applications. *Chemical Reviews* 2013, 113, 6734-6760.

[6] Fan, W.; Snyder, M.; Kumar, S.; Lee, P.; Yoo, W.; McCormick, A.; Penn, R.; Stein, A.; Tsapatsis, M. Hierarchical nanofabrication of microporous crystals with ordered mesoporosity. *Nature Materials* 2008, 7, 984-991.

[7] Awala, H.; Gilson, J.-P.; Retoux, R.; Boullay, P.; Goupil, J.-M.; Valtchev, V.; Mintova, S. Template-free nanosized faujasite-type zeolites. *Nature Materials* 2015, 14, 447-451.

[8] Valtchev, V.; Majano, G.; Mintova, S.; Perez-Ramirez, J. Tailored crystalline microporous materials by post-synthesis modification. *Chemical Society Reviews* 2013, 42, 263-290.

[9] Hartmann, M.; Machoke, A. G.; Schwieger, W. Catalytic test reactions for the evaluation of hierarchical zeolites. *Chemical Society Reviews* 2016, 45, 3313-3330.

[10] Smaihi, M.; Barida, O.; Valtchev, V. Investigation of the Crystallization Stages of LTA-Type Zeolite by Complementary Characterization Techniques. *European Journal of Inorganic Chemistry* 2003, 24, 4370-4377.

[11] Valtchev, V. Preparation of regular macroporous structures built of intergrown silicalite-1 nanocrystals. *Journal of Materials Chemistry* 2002, 12, 1914-1918.

[12] Tsapatsis, M. 2-dimensional zeolites. *AIChE Journal.* 2014, 60, 2374-2381.

[13] Corma, A.; Fornes, V.; Pergher, S. B.; Maesen, T. L. M.; Buglass, J. G. Delaminated zeolite precursors as selective acidic catalysts. *Nature* 1998, 396, 353-356.

[14] Choi, M.; Cho, H. S.; Srivastava, R.; Venkatesan, C.; Choi, D.-H.; Ryoo, R. Amphiphilic organosilane-directed synthesis of crystalline zeolite with tunable mesoporosity. *Nature Materials* 2006, 5, 718-723.

[15] Choi, M.; Na, K.; Kim, J.; Sakamoto, Y.; Terasaki, O.; Ryoo, R. Stable single-unit-cell nanosheets of zeolite MFI as active and long-lived catalysts. *Nature* 2009, 461, 246-249.

[16] Na, K.; Jo, C.; Kim, J.; Cho, K.; Jung, J.; Seo, Y.; Messinger, R. J.; Chmelka, B. F.; Ryoo, R.

Directing Zeolite Structures into Hierarchically Nanoporous Architectures. *Science* 2011, 333, 328-332.

[17] Zhang, X.; Liu, D.; Xu, D.; Asahina, S.; Cychosz, K. A.; Agrawal, K. V.; Al Wahedi, Y.; Bhan, A.; Al Hashimi, S.; Terasaki, O.; Thommes, M.; Tsapatsis, M. Synthesis of Self-Pillared Zeolite Nanosheets by Repetitive Branching, *Science* 2012, 336, 1684-1687.

[18] van Donk, S.; Janssen, A. H.; Bitter, J. H.; de Jong, K. P. Generation, Characterization, and Impact of Mesopores in Zeolite Catalysts. *Catalysis Reviews-Science and Engineering* 2003, 45, 297-319.

[19] Young D. A. Hydrocarbon conversion process and catalyst comprising a crystalline alumino-silicate leached with sodium hydroxide. US Pat. 3,326,797, assigned to Unocal, 1964.

[20] Gilson, J.-P.; Nanne, J. M.; Den Otter, G. J. Process for isomerizing hydrocarbons. EP 0398416, assigned to Shell, 1989.

[21] Milina, M.; Mitchell, S.; Crivelli, P.; Cooke, D.; Pérez-Ramírez, J. Mesopore quality determines the lifetime of hierarchically structured zeolite catalysts. *Nature Communications* 2014, 5, 3922.

[22] Valtchev, V.; Balanzat, E.; Mavrodinova, V.; Diaz, I.; El Fallah, J.; Goupil, J.-M. High Energy Ion Irradiation-Induced Ordered Macropores in Zeolite Crystals. *Journal of the American Chemical Society* 2011, 133, 18950-18956.

[23] Qin, Z.; Gilson, J.-P.; Valtchev, V. Mesoporous zeolites by fluoride etching. *Current Opinion in Chemical Engineering* 2015, 8, 1-6.

[24] Qin, Z.; Melinte, G.; Gilson, J.-P.; Jaber, M.; Bozhilov, K.; Boullay, P.; Mintova, S.; Ersen, O.; Valtchev, V. The Mosaic Structure of Zeolite Crystals. *Angewandte Chemie International Edition* 2016, 55, 15049-15052.

[25] Qin, Z.; Cychosz, K. A.; Melinte, G.; El Siblani, H.; Gilson, J.-P.; Thommes, M.; Fernandez, C.; Mintova, S.; Ersen, O.; Valtchev, V. Opening the Cages of Faujasite-Type Zeolite. *Journal of the American Chemical Society* 2017, 139, 17273-17276.

[26] Valtchev, V.; Gilson, J.-P.; Qin, Z. Method for the preparation of synthetic crystalline zeolite materials with enhanced total pore volume. WO 2016005783 A1, assigned to CNRS, 2016.

[27] Breck, D. W.; Skeels, G. W. Silicon substituted zeolite compositions and process for preparing same. U.S. Patent 4,503,023, assigned to Union Carbide. 1985.

[28] Skeels, G. W.; Breck, D. W. in *Proceedings of the Sixth International Zeolite Conference,* Olson, D.; Bisio, A. Eds.; Butterworths, Guildford, UK, 1984; p. 87.

[29] Chen, X.; Todorova, T.; Vimont, A.; Ruaux, V.; Qin, Z.; Gilson, J.-P.; Valtchev, V. In situ and post-synthesis control of physicochemical properties of FER-type crystals. *Microporous and Mesoporous Materials* 2014, 200, 334-342.

[30] Ajot, H.; Joly, J. F.; Lynch, J.; Raatz, F.; Caullet, P. Formation of Secondary Pores in Zeolites During Dealumination: Influence of The Crystallographic Structure and Of the Si/Al Ratio. In *Studies in Surface Science and Catalysis*, Rodriguez-Reinoso, F., Rouquerol, J., Sing, K. S. W., Unger, K. K., Eds.; Elsevier: 1991; Vol. 62, p 583-590.

[31] Lakiss, L.; Ngoye, F.; Canaff, C.; Laforge, S.; Pouilloux, Y.; Qin, Z.; Tarighi, M.; Thomas, K.; Valtchev, V.; Vicente, A.; Pinard, L.; Gilson, J.-P.; Fernandez, C. On the remarkable resistance to coke formation of nanometer-sized and hierarchical MFI zeolites during ethanol to hydrocarbons transformation. *Journal of Catalysis* 2015, 328, 165-172.

[32] Boltz, M.; Losch, P.; Louis, B.; Rioland, G.; Tzanis, L.; Daou, T. J. MFI-type zeolite nanosheets for gas-phase aromatics chlorination: a strategy to overcome mass transfer limitations. *RSC Advances* 2014, 4, 27242-27249.

[33] Thommes, M.; Kaneko, K.; Neimark Alexander, V.; Olivier James, P.; Rodriguez-Reinoso, F.; Rouquerol, J.; Sing K. S.W. Physisorption of gases, with special reference to the evaluation of surface area and pore size distribution (IUPAC Technical Report). *Pure and Applied Chemistry* 2015, 87, 1051-1069.

[34] Kortunov, P.; Vasenkov, S.; Kärger.; J. Valiullin, R.; Gottschalk, P.; Fé Elía, M.; Perez, M.; Stöcker, M.; Drescher, B.; McElhiney, G.; Berger, C.; Gläser, R.; Weitkamp, J. The role of mesopores in intracrystalline transport in USY zeolite: PFG NMR diffusion study on various length scales. *Journal of the American Chemical Society*, 2005, 127, 13055-13059.

[35] Groen, J. C.; Bach, T.; Ziese, U.; Paulaime-van Donk, A. M.; de Jong, K. P.; Moulijn, J. A.; Pérez-Ramírez, J. Creation of Hollow Zeolite Architectures by Controlled Desilication of Al-Zoned ZSM-5 Crystals. *Journal of the American Chemical Society*, 2005, 127, 10792-10793.

[36] Mei, C.; Liu, Z.; Wen, P.; Xie, Z.; Hua, W.; Gao, Z. Regular HZSM-5 microboxes prepared via a mild alkaline treatment. *Journal of Materials Chemistry*, 2008, 18, 3496-3500.

[37] Danilina, N.; Krumeich, F.; Castelanelli, S. A.; van Bokhoven, J. A. Where Are the Active Sites in Zeolites? Origin of Aluminum Zoning in ZSM-5. *The Journal of Physical Chemistry C*, 2010, 114, 6640-6645.

[38] Suga, M.; Asahina, S.; Sakuda, Y.; Kazumori, H.; Nishiyama, H.; Nokuo, T.; Alfredsson, V.; Kjellman, T.; Stevens, S. M.; Cho, H. S.; Cho, M.; Han, L.; Che, S.; Anderson, M. W.; Schüth, F.; Deng, H.; Yaghi, O. M.; Liu, Z.; Jeong, H. Y.; Stein, A.; Sakamoto, K.; Ryoo, R.; Terasaki, O. Recent progress in scanning electron microscopy for the characterization of fine structural details of nano materials. *Progress in Solid State Chemistry*, 2014, 42, 1-21.

[39] Wang, Y.; Lin, M.; Tuel, A. Hollow TS-1 crystals formed via a dissolution–recrystallization process. *Microporous and Mesoporous Materials*, 2007, 102, 80-85.

[40] Qin, Z.; Lakiss, L.; Gilson, J. P.; Thomas, K.; Goupil, J. M.; Fernandez, C.; Valtchev, V. Chemical Equilibrium Controlled Etching of MFI-Type Zeolite and Its Influence on Zeolite Structure, Acidity, and Catalytic Activity. *Chemistry of Materials* 2013, 25, 2759-2766.

[41] Anderson, M. W.; Agger, J. R.; Hanif, N.; Terasaki, O. Growth models in microporous materials. *Microporous and Mesoporous Materials*, 2001, 48, 1-9.

[42] Meza, L. I.; Anderson, M. W.; Agger, J. R.; Cundy, C. S.; Chong, C. B.; Plaisted, R. J. Controlling Relative Fundamental Crystal Growth Rates in Silicalite: AFM Observation. *Journal of the American Chemical Society*, 2007, 129, 15192-15201.

[43] Lupulescu, A. I.; Rimer, J. D. In Situ Imaging of Silicalite-1 Surface Growth Reveals the Mechanism of Crystallization. *Science*, 2014, 344, 729-732.

[44] De Yoreo, J. J.; Gilbert, P. U. P. A.; Sommerdijk, N. A. J. M.; Penn, R. L.; Whitelam, S.; Joester, D.; Zhang, H.; Rimer, J. D.; Navrotsky, A.; Banfield, J. F.; Wallace, A. F.; Michel, F. M.; Meldrum, F. C.; Cölfen, H.; Dove, P. M. Crystallization by particle attachment in synthetic, biogenic, and geologic environments. *Science*, 2015, 349, aaa6760.

[45] Lønstad Bleken, B.-T.; Mino, L.; Giordanino, F.; Beato, P.; Svelle, S.; Lillerud, K. P.; Bordiga, S. Probing the surface of nanosheet H-ZSM-5 with FTIR spectroscopy. *Physical Chemistry Chemical Physics* 2013, 15, 13363-13370.

[46] Derouane, E. G.; Nagy, J. B.; Dejaifve, P.; van Hooff, J. H. C.; Spekman, B. P.; Védrine, J. C.; Naccache, C. Elucidation of the mechanism of conversion of methanol and ethanol to hydrocarbons on a new type of synthetic zeolite. *Journal of Catalysis,* 1978, 53, 40-55.

[47] Meunier, F. C.; Verboekend, D.; Gilson, J.-P.; Groen, J. C.; Pérez-Ramírez, J. Influence of crystal size and probe molecule on diffusion in hierarchical ZSM-5 zeolites prepared by desilication. *Microporous and Mesoporous Materials*, 2012, 148, 115-121.

[48] Feller, A.; Guzman, A.; Zuazo, I.; Lercher, J. A. On the mechanism of catalyzed isobutane/butene alkylation by zeolites. *Journal of Catalysis,* 2004, 224, 80-93.

[49] Narbeshuber, T. F.; Brait, A.; Seshan, K.; Lercher, J. A. Dehydrogenation of Light Alkanes over Zeolites. *Journal of Catalysis,* 1997, 172, 127-137.

[50] Magnoux, P.; Roger, P.; Canaff, C.; Fouche, V.; Gnep, N. S.; Guisnet, M. New Technique for the Characterization of Carbonaceous Compounds Responsible for Zeolite Deactivation. In *Studies in Surface Science and Catalysis*, Delmon, B., Froment, G. F., Eds.; Elsevier: 1987; Vol. 34, p 317-330.

[51] Barbera, K.; Bonino, F.; Bordiga, S.; Janssens, T. V. W.; Beato, P. Structure–deactivation relationship for ZSM-5 catalysts governed by framework defects. *Journal of Catalysis* 2011, 280, 196-205.

[52] Thibault-Starzyk, F.; Vimont, A.; Gilson, J.-P. 2D-COS IR study of coking in xylene isomerisation on H-MFI zeolite. *Catalysis Today* 2001, 70, 227-241.

[53] Lee, K.; Lee, S.; Jun, Y.; Choi, M. Cooperative effects of zeolite mesoporosity and defect sites on the amount and location of coke formation and its consequence in deactivation. *Journal of Catalysis* 2017, 347, 222-230.

[54] Madeira, F. F.; Tayeb, K. B.; Pinard, L.; Vezin, H.; Maury, S.; Cadran, N. Ethanol transformation into hydrocarbons on ZSM-5 zeolites: Influence of Si/Al ratio on catalytic performances and deactivation rate. Study of the radical species role. *Applied Catalysis A: General* 2012, 443–444, 171-180.

[55] Ennaert, T.; Van Aelst, J.; Dijkmans, Jan.; De Clercq, R.; Schutyser, W.; Dusselier, M.; Verboekend, D.; Sels, B. F. Potential and Challenges of Zeolite Chemistry in the Catalytic Conversion of Biomass. *Chemical Society Reviews* 2016, 45, 584-611.

1

2

1 SYNOPSIS (Word Style “SN_Synopsis_TOC”).

2